From the UV to the static-field limit: rates and scaling laws of intense-field ionization of helium

Parker, J., Armstrong, G. S. J., Boca, M., & Taylor, K. (2009). From the UV to the static-field limit: rates and scaling laws of intense-field ionization of helium. Journal of Physics B: Atomic Molecular and Optical Physics, 42(13), 134011-134011. [134011]. DOI: 10.1088/0953-4075/42/13/134011

Published in:
Journal of Physics B: Atomic Molecular and Optical Physics

From the UV to the static-field limit: rates and scaling laws of intense-field ionization of helium

2009 J. Phys. B: At. Mol. Opt. Phys. 42 134011

(http://iopscience.iop.org/0953-4075/42/13/134011)

J. Phys. B: At. Mol. Opt. Phys. **42** (2009) 134011 (8pp) doi:10.1088/0953-4075/42/13/134011

From the UV to the static-field limit: rates and scaling laws of intense-field ionization of helium

J S Parker[1], G S J Armstrong[1], M Boca[2] and K T Taylor[1]

[1] Department of Applied Mathematics and Theoretical Physics, Queen's University Belfast, Belfast BT7 1NN, UK
[2] Faculty of Physics, University of Bucharest, 70709 Bucharest, Romania

Received 14 January 2009
Published 12 June 2009
Online at stacks.iop.org/JPhysB/42/134011

Abstract
We present high-accuracy calculations of ionization rates of helium at UV (195 nm) wavelengths. The data are obtained from full-dimensionality integrations of the helium-laser time-dependent Schrödinger equation. Comparison is made with our previously obtained data at 390 nm and 780 nm. We show that scaling laws introduced by Parker *et al* extend unmodified from the near-infrared limit into the UV limit. Static-field ionization rates of helium are also obtained, again from time-dependent full-dimensionality integrations of the helium Schrödinger equation. We compare the static-field ionization results with those of Scrinzi *et al* and Themelis *et al*, who also treat the full-dimensional helium atom, but with time-independent methods. Good agreement is obtained.

(Some figures in this article are in colour only in the electronic version)

1. Introduction

In a previous publication [1], we presented calculations of single-ionization rates of helium at two Ti-Sapphire laser wavelengths (390 nm and 780 nm). We showed that the scaling properties of the rates in intensity and wavelength could be described in terms of surprisingly simple laws that could be derived directly from ponderomotive-shifted perturbation theory: lowest-order perturbation theory in which the ionization potential is modified to increase linearly with intensity in order to correctly model the ponderomotive and Stark shifts.

In this paper, we extend the discussion with new calculations in both the high-frequency limit and the static-field limit. The first set of calculations was performed at UV wavelengths (195 nm) over an intensity range $0 < I < 32.0 \times 10^{14}$ W cm^{-2}. The second set of calculations was performed with static electric fields in the range $0 < E < 0.4$ au. In both cases, single-electron ionization rates were obtained from the numerical integration of the full-dimensional time-dependent Schrödinger equation as described in [1, 2]. The new data allow us to refine and extend the discussion of scaling laws introduced in [1]. As we shall see, the conclusions of [1] are largely confirmed by the new data.

We begin the discussion with figure 1, a plot of the new and the old results in the lower intensity range $0 < I < 16.0 \times 10^{14}$ W cm^{-2}. Preliminary discussion of figure 1 will serve as an introduction to a more detailed dicussion in the succeeding sections. The helium atom is initially in its lowest energy state. Bound-state resonances are smoothed away to clarify the general trend of the rate curves, as described in [1]. In section 3, unsmoothed data are presented.

The most prominent feature of figure 1 is the vertical displacement of the rate curves. In sections 2 and 3, we derive a formula for the displacement in terms of atomic parameters and laser parameters. The frequency dependence of the displacement is found to be a consequence of the fact that the ionization in this limit is a multiphoton process, which to good approximation obeys a power law, Rate$(I) \sim [(d_0 E)^2]^N$ where E is the electric field, d_0 an effective dipole moment and N is the minimum number of photons required to free an electron from a ponderomotive shifted ionization potential. The vertical displacement (from the static results) divided by the laser frequency squared has a near linear dependence on the derivative of the ponderomotive shift with respect to the laser intensity.

The cycle-averaged static rates shown in figure 1 are obtained by averaging static-field rates over the range of

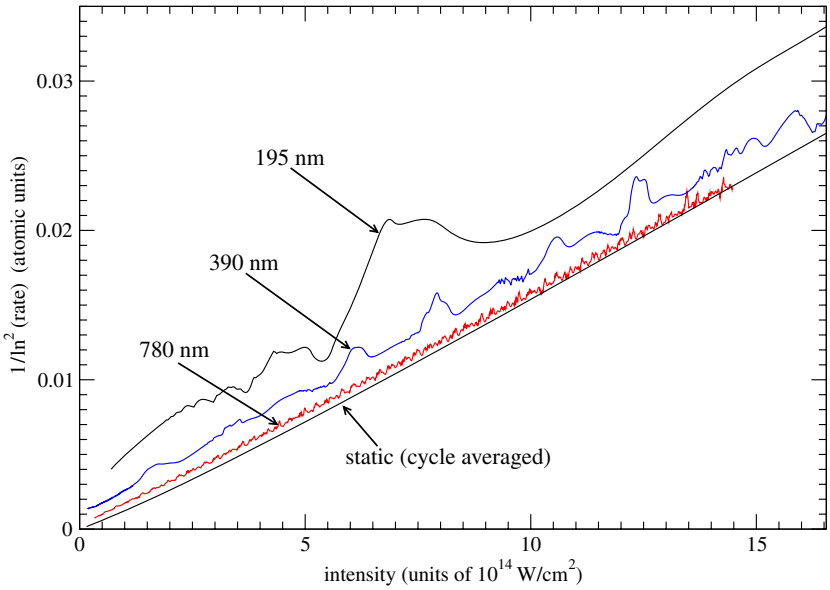

Figure 1. Single-ionization rates of helium obtained from numerical integration of the full-dimensional time-dependent Schrödinger equation. Multiphoton rates at 195 nm, 390 nm and 780 nm are shown, along with cycle-averaged static-field rates.

electric field strengths occurring in sinusoidally oscillating electric fields. More precisely, the sinusoid is modelled as a series of constant-strength (static) electric fields, (rectangles under the sinusoid curve), and the ionization yields predicted by static-field calculations are summed for each rectangle to calculate the total ionization yield expected over a field period. The result is translated into a rate (yield per field period divided by field period), which is plotted in figure 1 against the time-averaged intensity of the corresponding sinusoidal E-field. The cycle averaging described above produces the same result for any frequency sinusoid, but the resulting cycle-averaged rates will not be physically valid for fields that vary so rapidly that the atomic response is not adiabatic. The adiabatic limit is discussed further in section 4.

A striking feature of figure 1 is the clear space between the near infrared ionization results (780 nm) and the static-field results. Although it is difficult to see on the scale of figure 1, the 780 nm rates exceed the static rates by factors of 100, 8, 3 and 2 at intensities of $I = 1$, 2, 3 and 4×10^{14} W cm^{-2}, respectively. But we also see that the 780 nm results appear to begin merging with the static ionization results in the high intensity limit, $I > 14.0 \times 10^{14}$ W cm^{-2}.

The intensity $I = 14.0 \times 10^{14}$ W cm^{-2}, which is associated with a peak E-field of 0.2 au, is the threshold intensity for the onset of above-barrier ionization (ABI) according to Scrinzi *et al* [3]. ABI is an intense-field process in which the electric field suppresses the Coulomb potential to the extent that the electron (originally in the ground state) can escape without tunnelling. ABI is also referred to as barrier-suppression ionization (BSI). Several different methods have been considered for estimating the onset of ABI [3, 5–8], with estimates for helium generally in the 0.2 au–0.4 au range. In our static-field results we identify two interesting transition points: $E = 0.175$ au and $E = 0.38$ au. For field strengths $E < 0.38$ au the helium atom responds adiabatically to electric fields that are ramped on sufficiently gently. However, above $E = 0.38$ au we have difficulty producing a clear adiabatic response for any length of ramp-on. At $E = 0.175$ au, the static-ionization rate curve $\Gamma(E)$ undergoes a change in a functional form, with the abrupt appearance of a rapidly increasing component that scales as E^4. In section 4, we discuss the calculation of static-field ionization rates and the adiabatic response of helium to slowly varying electric fields.

2. Derivation of scaling laws

In [1], we showed that helium intense-field ionization rates obey simple scaling laws in intensity and frequency. In [1], the discussion was limited to optical wavelengths. The scaling laws were inferred from a perturbative description of ionization which successfully modelled ionization rates over an intensity range that extended to an order of magnitude higher than the usual lowest order perturbation theory with a static potential. In this section, we review the findings of [1] in preparation for the analysis of new data in section 3.

Figure 2 shows the 390 nm results along with the result of a curve fit based on the classic perturbative power law I^N. We write this as

$$\Gamma(I) = A\left(d_0^2 I\right)^N. \tag{1}$$

Here N, the exponent of I, is set to 8, the minimum number of photons required to ionize. The ionization potential is assumed to be static so that the exponent is a constant.

Next we introduce a ponderomotive-shifted ionization potential [1] into the power law. We again restrict the calculation to 390 nm, $\omega_{390} = 0.116\,83$ au. Intensity I will always be written in units of 10^{14} W cm^{-2}. With intensity I in these units, the ponderomotive shift in au, $U_p(I, \omega)$, is $(0.053\,36)^2 I (4\omega^2)^{-1}$, where ω is in au. Setting $\omega = 0.116\,83$ au and writing U_p in units of $\omega_{390} = 0.116\,83$ au, we get $U_p = 0.4464I = \xi_0 I$. Henceforth, we add on to the ponderomotive

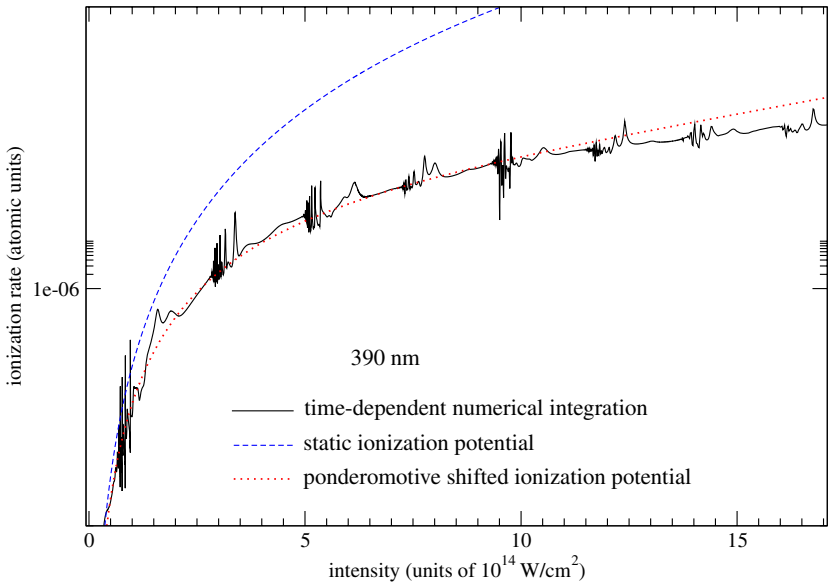

Figure 2. Single-ionization rates of helium at 390 nm as a function of intensity. Rates obtained from numerical integration are compared with those obtained using equations (1) and (2).

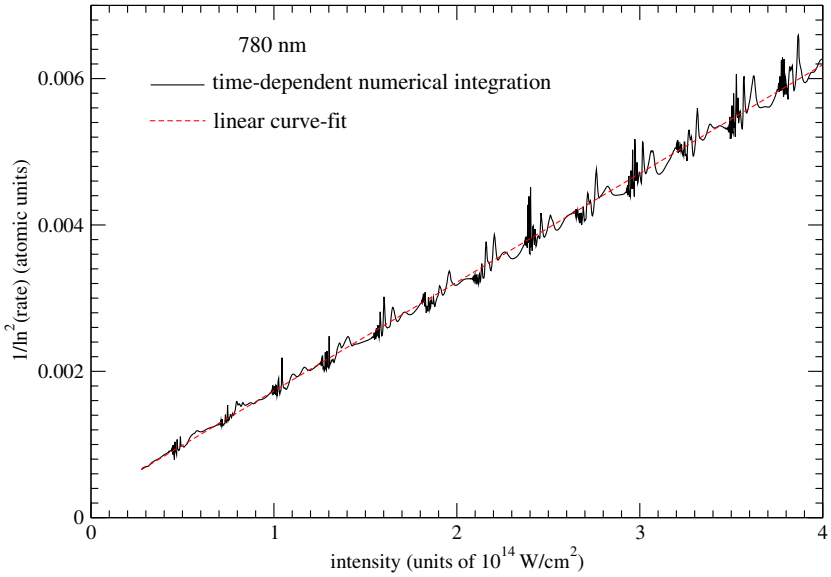

Figure 3. Single-ionization rates of helium at 780 nm as a function of intensity.

shift a small second-order Stark shift (Stark $= \xi_2 I = 0.0096 I$) and write $\xi = \xi_0 + \xi_2 = 0.456$. (The value of the second-order Stark shift is obtained from an analysis of intensity dependence of the positions of the resonance peaks visible in figures 3–5.) The ionization potential in units of the 390 nm photon is now $N_0(I) = (I_p + U_p(I) + \xi_2 I)/0.11683 = n + \xi I$, where $n = 7.735$ and $\xi = 0.456$. Using these parameters, Γ takes the form

$$\Gamma(I) = A\left(d_0^2 I\right)^{N_0(I)}. \tag{2}$$

Figure 2 shows the 390 nm rate data along with the results of equations (1) and (2). The constants $A = 548\,000.0$ and $d_0 = 0.138$ were chosen to fit equation (2) to non-resonant features of the 390 nm data. The power law formula works well over the range $I = 0.5$ to 9×10^{14} W cm^{-2}, an order of magnitude higher in intensity than the static-potential perturbation theory of equation (1), evidence that the ionization process is a multiphoton process rather than tunnelling or ABI.

Suppose we now attempt to use the 390 nm results to predict 780 nm ionization rates. In the weak-field limit, twice as many photons are now required for ionization. As a first step then, we would double the exponent of intensity: $\left(d_0^2 I\right)^{N_0}$ becomes $\left(\left(d_0^2 I\right)^{N_0}\right)^R$ where R is wavelength in units of 390 nm. In the 780 nm case $R = 2$. However this fails in the intense field limit, because $N_0 R$ underestimates the number of photons required for ionization in the 780 nm case: the

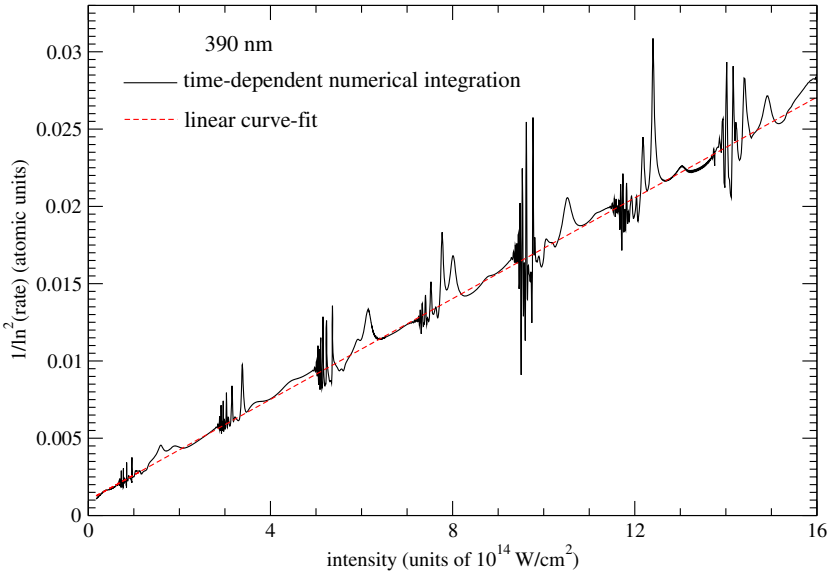

Figure 4. Single-ionization rates of helium at 390 nm as a function of intensity.

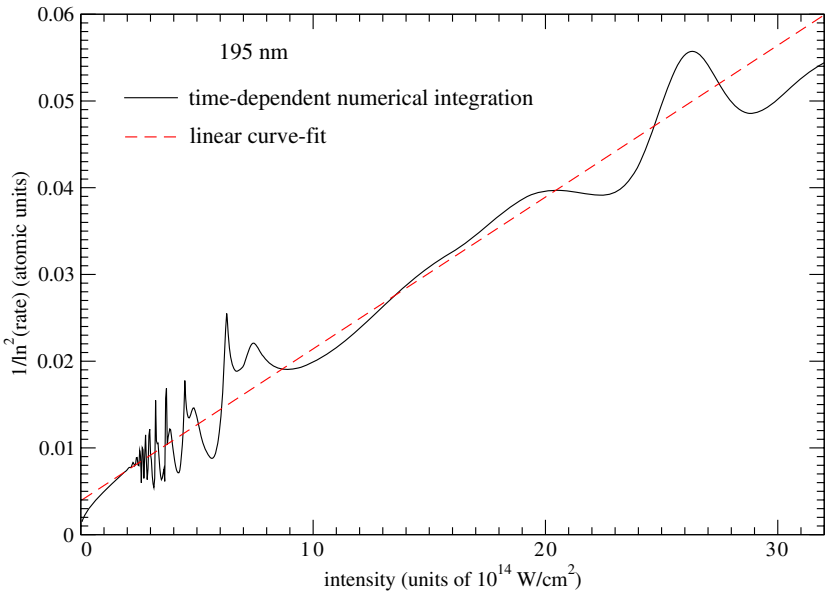

Figure 5. Single-ionization rates of helium at 195 nm.

ponderomotive shift in the 780 case is four times that in the 390 nm case for any given intensity. As discussed in [1], the solution is to use a scaled intensity, $\bar{I} = IR^2$. Changing variables to $\bar{I}$ in equation (1) yields

$$\Gamma(\bar{I}, R) = \left[\frac{A}{R}\left(d_0^2\bar{I}\right)^{N_0(\bar{I})}\right]^R. \tag{3}$$

If this new variable, $\bar{I}$, is held constant, then equation (3) describes ionization from a potential well whose depth remains constant as the wavelength R is varied explicitly. Equation (3) models the 780 nm data well [1], over the same intensity range attained by equation (2) in figure 1, provided the scaled intensity $\bar{I}$ is used, and provided A is divided by the scaled wavelength R, as written in equation (3).

The A/R term of equation (3) was explored only briefly in [1]. Although it is separate from the effective dipole d_0, its variation in R reflects the fact that the effective dipole should not really be constant as R varies. As we show in the following section, it can be regarded as a rather small wavelength dependence in the atomic parameters, and in figure 1 it manifests itself as the slight R dependence in the slopes of the ionization curves. We consider it to be of some importance though, since interpolation of the results at values of R between $R = 2$ and $R = 0.5$ should be useful to experimentalists. In the following section, we show that using equation (3) (via A/R) to interpolate between $R = 1$ and $R = 0.5$ introduces some error, and a better method will be discussed.

3. Application of scaling laws at 195 nm, 390 nm and 780 nm

The perturbative power laws of the previous section clarify the frequency scaling of $\Gamma(I)$, but several features of the rate curves that are clearly apparent in figure 1 are not as apparent in the power law of equation (3). In particular, in figure 1 the vertical displacements of the rate curves (above the static results) scale as the square of the laser frequency (ω^2). Additionally, on the scale of figure 1 the curves are nearly linear in their general trend. The ω^2 displacement is of particular interest since it distinguishes laser-driven ionization from static-field ionization. Below, we derive a formula for this ω^2 displacement in terms of constants associated with the ponderomotive shift and the second-order Stark shift (ξ), as well as d_0, A, and wavelength.

We begin by writing $\Gamma(I)$ in a functional form which agrees with the power law formulations over a certain interval (from $\bar{I} = 1$ to about 8) and retains the scaling behaviour, but makes explicit the two characteristics of the rate curves described in the above paragraph. The new functional form is useful in the high intensity limit and as we will see has additional practical advantages. The functional form is

$$\Gamma(I) = \exp\left(-\frac{1}{\sqrt{b_0 + b_1 I}}\right), \tag{4}$$

which is simply an expression of the observation that the (non-static) data shown in figure 1 are linear in their general trend. Since, over a certain interval of I, this curve fit coincides to good approximation with the power law equation (3), we immediately obtain b_0 and b_1 in terms of atom plus laser parameters d_0, A, n, R and ξ by exponentiating the natural log of equation (3) and equating exponents in equations (3) and (4):

$$b_0 R^2 + b_1 \bar{I} \simeq \left[\ln(A/R) + \ln\left(d_0^2 \bar{I}\right)(n + \xi \bar{I})\right]^{-2}. \tag{5}$$

Choosing two values of $\bar{I}$ in equation (5) gives two linear equations in b_0 and b_1. But since the agreement between equations (3) and (4) is approximate, each different choice of the intensity pair $(\bar{I}_1, \bar{I}_2)$ will yield a somewhat different value for the pair (b_0, b_1). For most choices of $(\bar{I}_1, \bar{I}_2)$ however, (for example with $1.0 \leqslant \bar{I} < 4.0$) the derived values of (b_0, b_1) differ little from each other, varying by only a few per cent. Setting $(\bar{I}_1, \bar{I}_2) = (1, 2)$ gives the simplest expression for b_0:

$$b_0 R^2 = 2\left[\ln(A/R) + \left(\ln\left(d_0^2\right)(n + \xi)\right]^{-2} - \left[\ln(A/R) + \ln\left(2d_0^2\right)(n + 2\xi)\right]^{-2}. \tag{6}$$

Using the atomic and laser parameters from the previous section ($A = 548\,000$, $d_0 = 0.138$, $n = 7.735$, $\xi = 0.456$), we can compare equation (6) with calculated results for $\lambda =$ 780 nm, 390 nm and 195 nm ($R = 2$, 1 and 0.5, respectively).

In figures 3–5, we plot calculated ionization rates over an intensity range $0.0 < \bar{I} < 16.0$, for $R = 2$ (780 nm) and $R = 1$ (390 nm). At $R = 0.5$ (195 nm) $\bar{I} < 8.0$, because the data end at $I = 32.0 \times 10^{14}$ W cm^{-2} (recall $\bar{I} = IR^2$). The ordinate in each of the figures is $1/\ln^2(\Gamma(I))$, so that the straight lines appearing in the figures correspond directly to the $b_0 + b_1 I$ term that appears in equation (4). The ordinate intercept of the straight lines drawn in figures 3–5 is the value of b_0 predicted by the numerically integrated ionization rates. The coefficient b_0, then, is the quantity we originally set out to derive in terms of atom plus laser parameters: the vertical displacement of the ionization curves in figure 1. We find below that b_0 is, to very good approximation, linear in ω^2, (or $1/R^2$, recalling that R is wavelength in units of 390 nm). The values of b_0 derived from figures 3–5 are as follows:

$$780 \text{ nm } (R = 2.0) : b_0 = 0.000\,247,$$
$$390 \text{ nm } (R = 1.0) : b_0 = 0.000\,990,$$
$$195 \text{ nm } (R = 0.5) : b_0 = 0.003\,920.$$

The values of b_0 derived from equation (6) are as follows:

$$780 \text{ nm } (R = 2.0) : b_0 = 0.000\,250,$$
$$390 \text{ nm } (R = 1.0) : b_0 = 0.000\,989,$$
$$195 \text{ nm } (R = 0.5) : b_0 = 0.003\,856.$$

The good agreement suggests that equation (6) can be regarded as qualitatively correct even outside the frequency range used in its derivation ($R = 1$ to $R = 2$). As an application, equation (6) may now be used to explore sensitivity of $a_0 = b_0 R^2$ to changes in the atom plus laser parameters. Over a wider range of frequencies, values $a_0 = b_0 R^2$ given by equation (6) are as follows:

$$3120 \text{ nm } (R = 8.0) : a_0 = 0.000\,993,$$
$$1560 \text{ nm } (R = 4.0) : a_0 = 0.001\,000,$$
$$780 \text{ nm } (R = 2.0) : a_0 = 0.001\,000,$$
$$390 \text{ nm } (R = 1.0) : a_0 = 0.000\,989,$$
$$195 \text{ nm } (R = 0.5) : a_0 = 0.000\,964.$$

Although a_0 is insensitive to wavelength, it is sensitive to each of the other parameters. For example, in the $R = 1$ case, one may easily verify numerically that a_0 is very nearly linear in ξ. If ξ were half its actual value of 0.456 then a_0 at $R = 1$ would be reduced by half to 0.000 51. At $R = 2$, a_0 would be reduced to 0.0006, and at $R = 0.5$ it would be reduced to 0.000 38. The vertical separation (on the scale of figure 1), then gives us a measure of the derivative of the ponderomotive shift (plus Stark shifts) with respect to intensity: ξ. The frequency squared dependence of the actual separation, $b_0 = a_0/R^2$, arises because the rate curves follow the familiar power law of multiphoton ionization: the minimum number of photons to ionize scales linearly with wavelength, so that R appears in the exponent of the power law. ξ does not appear in the theory of static-field ionization, and therefore sensitivity to ξ distinguishes laser-driven ionization processes from static.

Equation (6) predicts a large change in a_0 in response to a small change in the scaled ionization potential $n = I_p/0.116\,83$. For example, n at 6.7832 (for neon) is about 13% smaller than n for helium (7.735), but the resulting a_0 is 0.001 39 at $R = 2$, a 39% increase. At the neon value of n, the R dependence in a_0 is again weak, hence an (approximate) ω^2 displacement of rate curves would again be observed, as in figure 1.

We cannot regard equation (6) as quantitatively accurate, because as we discuss below, wavelength dependence introduced by the A/R term is found to be in error by about 10% at $R = 0.5$. Evidently, equation (6) works well over the

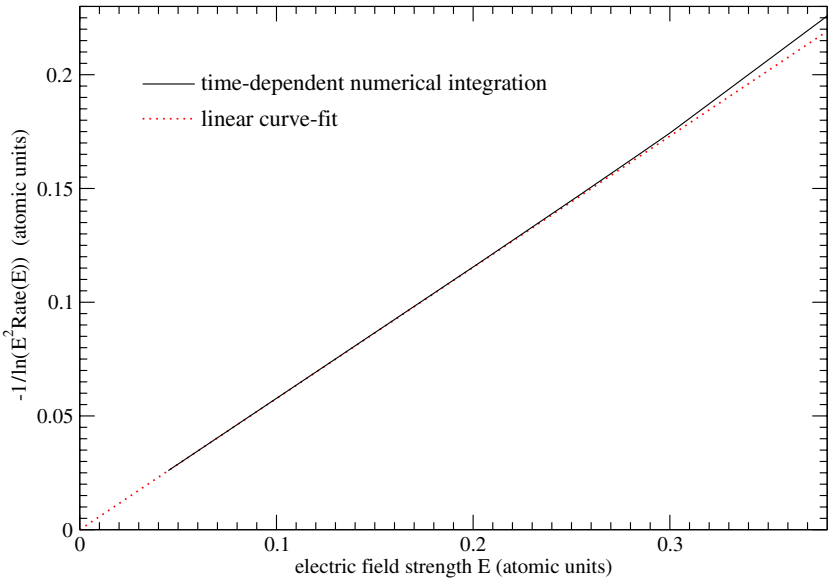

Figure 6. Single-ionization rates $(-1/\ln(E^2\ \mathrm{Rate}(E)))$ of helium induced by static electric field E. Rates are in au.

range that it can be tested ($R = 0.5$–2) because it is insensitive to the A/R term, $R \geqslant 0.5$.

We can learn more about the relation between A/R and the straight-line parameters of equation (4) by repeating the above exercise for the slope b_1 rather than b_0. First, the values of b_1 derived from figures 3–5 are as follows:

$$780\ \text{nm}\ (R = 2.0) : b_1 = 0.001\,485,$$
$$390\ \text{nm}\ (R = 1.0) : b_1 = 0.001\,630,$$
$$195\ \text{nm}\ (R = 0.5) : b_1 = 0.001\,750.$$

The values of b_1 derived from equation (5) using $(\bar{I}_1, \bar{I}_2) = (1, 3)$ are as follows:

$$780\ \text{nm}\ (R = 2.0) : b_1 = 0.001\,470,$$
$$390\ \text{nm}\ (R = 1.0) : b_1 = 0.001\,680,$$
$$195\ \text{nm}\ (R = 0.5) : b_1 = 0.001\,930.$$

The pair $(\bar{I}_1, \bar{I}_2) = (1, 3)$ minimizes error at $R = 1$ and 2, but the 10% error at $R = 0.5$ stands out. In fact, all of the variation in b_1 observed as R varies from 0.5 to 2 is a result of the A/R term (R appears nowhere else), so we know immediately that the purpose of the A/R term in equation (3) is to model this slight wavelength dependence in b_1. From the above data, we learn that it does not succeed at this with quantitative accuracy. In [1], we added an additional R dependence to d_0, which worked well. In fact, on physical grounds we should expect the effective dipole moment d_0 to vary with R and perhaps intensity also, as discussed in [1]. But this variation is not understood well enough to provide guidance on interpolating the above results to new values of R, especially in the 0.5–1.0 range.

Turning to the problem of interpolating the above results to new values of R, we must say, then, that this is an unsolved problem. Purely on numerical grounds though, it appears that equation (4) is best suited for this interpolation: the numerically determined b_1 is roughly constant, with a modest correction that is, to first approximation, linear in $\ln(R)$. The perturbative power law of equation (3), by contrast, was originally formulated to provide theoretical guidance on the dominant scaling parameters of the ionization process.

For completeness, we write the three curve fits to the three straight (dashed) lines in figures 3–5. (Here $a_0 = b_0 R^2$ and $a_1 = b_1$.) We have

$$\Gamma(\bar{I}, R) = \exp\left(-\frac{R}{\sqrt{a_0 + a_1 \bar{I}}}\right), \tag{7}$$

where Γ is in au and $I = \bar{I}/R^2$ is in units of 10^{14} W cm^{-2}. The values of a_0 and a_1 derived from figures 3–5 are as follows:

$$780\ \text{nm}\ (R = 2.0) : a_0 = 0.000\,9882, \qquad a_1 = 0.001\,485,$$
$$390\ \text{nm}\ (R = 1.0) : a_0 = 0.000\,9900, \qquad a_1 = 0.001\,630,$$
$$195\ \text{nm}\ (R = 0.5) : a_0 = 0.000\,9800, \qquad a_1 = 0.001\,750.$$

Here intensity is limited to $\bar{I} < 16$ for 390 nm and 780 nm (and $\bar{I} < 8$ for 195 nm). Over higher intensity ranges, the curves given in equation (5) of [1] may be used.

Finally, we call attention to an important feature of figure 5 that has not yet been discussed. For sufficiently small intensities, the straight line fit associated with the multiphoton rate curves of figures 3–5 fails. It fails because as intensity approaches zero, the result from the power law of equation (3) approaches zero, whereas $\Gamma(\bar{I})$ of equation (7) does not. The disagreement is difficult to see in figures 3 and 4 (780 nm and 390 nm), but it is clear in figure 5 (195 nm). From figure 5 we conclude that at 195 nm the failure of equation (7) is unmistakable for $I < 1.0 \times 10^{14}$ W cm^{-2}. Close examination of the 390 nm data suggests that the corresponding threshold at 390 nm is 0.25×10^{14} W cm^{-2}.

4. Static-field ionization rates derived from time-dependent quantum mechanics

In figure 1, we presented static-field ionization rates that were averaged over the distribution of E-fields found in a

Table 1. Static-field ionization rates from the ground state of helium as a function of peak electric field strength E.

		Γ (au)		
E (au)	Present work	Scrinzi *et al* [3]	Themelis *et al* [4]	ADK theory [9]
0.045	9.4463×10^{-15}			1.75×10^{-14}
0.048	9.0006×10^{-14}			1.61×10^{-13}
0.05	3.3536×10^{-13}			6.10×10^{-13}
0.055	6.7817×10^{-12}			1.11×10^{-11}
0.06	7.8936×10^{-11}			1.23×10^{-10}
0.067	1.4045×10^{-9}		1.6×10^{-9}	1.96×10^{-9}
0.068	1.8365×10^{-9}		2.0×10^{-9}	2.78×10^{-9}
0.07	3.6360×10^{-9}		3.6×10^{-9}	5.42×10^{-9}
0.075	1.6945×10^{-8}		1.42×10^{-8}	2.45×10^{-8}
0.08	6.2093×10^{-8}	4.63×10^{-8}	5.57×10^{-8}	9.15×10^{-8}
0.09	5.3387×10^{-7}	5.09×10^{-7}	5.23×10^{-7}	8.20×10^{-7}
0.095	1.3413×10^{-6}		1.30×10^{-6}	2.06×10^{-6}
0.10	2.9391×10^{-6}	2.88×10^{-6}	2.92×10^{-6}	4.71×10^{-6}
0.11	1.1755×10^{-5}	1.15×10^{-5}	1.17×10^{-5}	1.96×10^{-5}
0.12	3.6829×10^{-5}	3.62×10^{-5}	3.66×10^{-5}	6.42×10^{-5}
0.13	9.5748×10^{-5}	9.43×10^{-5}	9.50×10^{-5}	1.74×10^{-4}
0.14	2.1495×10^{-4}	2.12×10^{-4}	2.13×10^{-4}	4.09×10^{-4}
0.15	4.2913×10^{-4}	4.23×10^{-4}	4.25×10^{-4}	8.56×10^{-4}
0.16	7.7875×10^{-4}	7.68×10^{-4}	7.70×10^{-4}	1.63×10^{-3}
0.18	2.0578×10^{-3}	2.03×10^{-3}	2.03×10^{-3}	4.73×10^{-3}
0.20	4.3347×10^{-3}	4.31×10^{-3}	4.30×10^{-3}	1.07×10^{-2}
0.225	9.0115×10^{-3}			2.57×10^{-2}
0.25	1.5793×10^{-2}	1.57×10^{-2}	1.56×10^{-2}	5.02×10^{-2}
0.30	3.5857×10^{-2}	3.56×10^{-2}	3.52×10^{-2}	1.35×10^{-1}
0.34	5.7545×10^{-2}	5.72×10^{-2}		2.40×10^{-1}
0.3773	8.1210×10^{-2}			3.65×10^{-1}
0.40		9.77×10^{-2}	9.64×10^{-2}	4.53×10^{-1}

sinusoidally oscillating field. In this section, we discuss static-field rates without the cycle averaging and present an analytical curve fit to the data.

In practice, the calculation of static-field ionization rates using the time-dependent Schrödinger equation is little different from the calculation of laser-driven ionization, which is described in detail in [1]. The E-field is ramped on smoothly to a peak value $E_{\max}$ using a sinusoidal profile: $E = E_{\max}(1 - \cos(\Omega t))/2$ for $0 < t < \pi/\Omega$. The integration is a finite-difference scheme in radial variables with a basis set of coupled spherical harmonics [2]. The integrations were repeated with increasingly large values for the maximum angular momenta $L_{\max}$ and ramp-on times T, until no change was observed in the final results. In the low E-field limit, the maximum total angular momentum of the two-electron partial waves was $12\hbar$. In the high E-field limit ($E > 0.25$ au), $24\hbar$ was used. The finite-difference grid introduces a detectable source of error in the calculations. Initially, all calculations were performed using a grid spacing δr of 0.29 au. Reducing δr to 0.2 au altered ionization rates by 0.3% at $E = 0.1$ au and by 0.03% at $E = 0.3$ au. Rates were obtained by measuring the rate of decay of population within a sphere of 18 Bohr radii about the atomic core. Perfect exponential decay was observed in this quantity at every choice of $E_{\max}$, provided the ramp-on of the E-field was sufficiently gentle.

The time-dependent approach was successful because an adiabatic response was observed for sufficiently slowly varying ramp-on profiles. More precisely, for sufficiently large ramp-on times, $T_a = \pi/\Omega_a$, all ramp-ons $T > T_a$ produced the same final ionization rate, and ionization adiabatically followed the slowly varying E-field. Translating $2\pi/\Omega_a$ into nanometres, we found $2\pi/\Omega_a$ at $E = 0.05$ au to be 4600 nm. At $E > 0.08$ au, we were able to use a shorter ramp-on: $2\pi/\Omega_a = 1150$ nm. At the highest field strengths, $E > 0.30$ au, it was again necessary to lengthen the ramp-on, using values of Ω_a such that $2\pi/\Omega_a = 2200$ nm. No adiabatic response was observed for $E > 0.38$ au. In other words each choice of ramp-on seemed to produce a different atomic response and a different ionization rate. Despite this source of uncertainty, at $E = 0.40$ au the measured ionization rate differed from Scrinzi's by only a few per cent.

Figure 6 shows the results of the helium static-field ionization rate calculations. The rate values are plotted as $-1/\ln(E^2\text{Rate}(E))$. The resulting curve is linear on the scale of figure 6 at E-field values below about 0.2 au. Above 0.25 au, the onset of a new profile is clearly visible to the eye.

Based on these considerations, the calculated data can be fit with a very simple function

$$\Gamma(E) = \frac{1}{E^2}\exp\left(-\frac{1}{1.47 \times 10^{-5} + 0.577E}\right) + 6.183(E - 0.1755)^4\text{Step}(E - 0.1755), \quad (8)$$

where the function Step $(x) = 1$ for $x > 0$, and 0 otherwise. Here $E < 0.4$ au. The E-field strength is in atomic units, as is $\Gamma(E)$. The numerical model (equation (8)) suggests that a

useful functional form for representing the behaviour of $\Gamma(E)$ for $E > 0.17$ au is a term that scales as E^4. However, the E^4 model is based on only five data points. The Scrinzi data [3] agree well with our data in the $0.2 < E < 0.4$ limit, although the Scrinzi data appear more consistent with an E^2 model for $E \gg 0.4$. The interesting feature of the E^4 model is that it commences abruptly at about $E = 0.175$ au. It is not well represented by, for example, a fourth-order polynomial that begins near $E = 0$.

To get an empirical formula for the cycle-averaged static rates shown in figure 1, multiplying equation (8) by $0.146I^{0.25}$ works well for $I < 50.0 \times 10^{14}$ W cm^{-2}, ($E < 0.3773$). (E in au is transformed into intensity in units of 10^{14} W cm^{-2} by $I = 14.0484(E/0.2)^2$.)

In table 1, we present our static results along with those of [3] and [4]. Both of the latter are based on full-dimensional solutions of the time-independent Schrödinger equation. The agreement between the full-dimensional methods is generally good. Agreement between the three highly dissimilar computational and theoretical methods does much to improve confidence in the results and methods. The classical ADK rate formula fails to model the ionization data in any limit we have considered. The ADK formula used here is discussed in [1]. Part of its failure arises from the fact that the classical ADK approximation is derived for one-electron atoms, not helium. The ADK approximation is the first term of a series solution for static-field ionization and works rather well under the restrictions assumed in its derivation: the weak static-field ionization of hydrogenic atoms [4].

5. Discussion

Only in recent years has it become possible to treat with quantitative rigour the response of helium (or any two-electron atomic system) to intense light [10–18]. In this paper, we presented calculations of helium single-ionization rates, $\Gamma(I)$, from the UV to the static-field limit. A full-dimensional treatment of the helium-laser interaction was a requirement for quantitative accuracy. Plotted together in figure 1 as $1/\ln^2(\Gamma(I))$ against intensity I, the data revealed a number of similarities and dissimilarities that could be explained in terms of scaling laws derived from ponderomotive-shifted perturbation theory.

We conclude by reviewing some of the more puzzling features of ionization encountered in the above discussion. The problem of estimating the onset of above-barrier ionization and of quantifying the relative contributions of tunnelling and ABI to a static ionization rate remains unsolved. ABI is inherently a classical concept. It may be defined as the limit in which an atom can ionize without tunnelling. Because it is possible to formulate any number of plausible but highly dissimilar classical models of ionization, estimates of the intensity threshold of ABI vary by a factor of over 4 [3, 5–8]. The Scrinzi estimate of 14×10^{14} W cm^{-2} ($E = 0.2$ au) is in the low range of published estimates.

Similarly, determining the exact contribution of tunnelling to ionization is an important theoretical problem that remains poorly understood. Let us consider the problem at 780 nm. Tunnelling is a static-field process. Its magnitude is therefore bounded by the static-field rates shown in figure 1. It is clear then that tunnelling does not contribute significantly to laser-driven ionization (780 nm) for $I < 4 \times 10^{14}$ W cm^{-2}. The static-field rates are too small by anything from a factor of 1000 in the low intensity range to a factor of 2 at 4×10^{14} W cm^{-2}. For intensities greater than 14×10^{14} W cm^{-2} it is increasingly likely that ABI dominates, although this limit is also poorly understood quantitatively. Tunnelling is too small to fully explain the 780 nm rates for 4×10^{14} W cm^{-2} $< I < 14 \times 10^{14}$ W cm^{-2}. In this range, we find that the ionization peaks associated with resonance that occur in the high-intensity limit differ little from corresponding resonant ionization features in the low-intensity limit (seen most clearly in figure 3). In both the low end and the high end, resonant behaviour is the signature of multiphoton ionization, and no static process can model the resonant rates. On the other hand, in the range 4×10^{14} W cm^{-2} $< I < 14 \times 10^{14}$ W cm^{-2} the static rates are a significant percentage of the non-resonant 780 nm rates. In fact, the static rates may be up to 80% of the non-resonant 780 nm rates in the high end of this intensity range. We do not believe that there is currently any reliable method of estimating the relative contributions of tunnelling, ABI and multiphoton ionization in this limit.

Acknowledgments

This work was supported in part by the UK Engineering and Physical Sciences Research Council and by the Northern Ireland Department of Employment and Learning.

References

[1] Parker J S, Meharg K J, McKenna G A and Taylor K T 2007 *J. Phys. B: At. Mol. Opt. Phys.* **40** 1729
[2] Smyth E S, Parker J S and Taylor K T 1998 *Comput. Phys. Commun.* **114** 1
[3] Scrinzi A, Geissler M and Brabec T 1999 *Phys. Rev. Lett.* **83** 706
[4] Themelis S I, Mercouris T and Nicolaides C A 1999 *Phys. Rev.* A **61** 024101
[5] Bauer D and Mulser P 1998 *Phys. Rev.* A **59** 569
[6] Tong X M and Lin C D 2005 *J. Phys. B: At. Mol. Opt. Phys.* **38** 2593
[7] Görlinger J, Plagne L and Kull H J 2000 *Appl. Phys.* B **71** 331
[8] Chardonnet C 1983 *PhD Thesis* L'Université Pierre et Marie Curie
[9] Ammosov M V, Delone N B and Krainov V P 1986 *Zh. Eksp. Teor. Fiz.* **91** 2008
[10] Glass D H and Burke P G 1999 *J. Phys. B: At. Mol. Opt. Phys.* **32** 407
[11] van der Hart H W, Doherty B J S, Parker J S and Taylor K T 2005 *J. Phys. B: At. Mol. Opt. Phys.* **38** L207
[12] Mercouris Th, Dionissopoulou S and Nicolaides C A 1997 *J. Phys. B: At. Mol. Opt. Phys.* **30** 4751
[13] Uiterwaal C J G J, Xenakis D, Charalambidis D, Maragakis P, Schröder H and Lambropoulos P 1998 *Phys. Rev.* A **57** 392
[14] Nikolopoulos L M M and Lambropoulos P 2001 *J. Phys. B: At. Mol. Opt. Phys.* **34** 545
[15] Trombetta F, Basile S and Ferrante G 1989 *J. Mod. Opt.* **36** 891
[16] Dundas D 2002 *Phys. Rev.* A **65** 023408
[17] Veniard V, Taieb R and Maquet A 2003 *Laser Phys.* **13** 465–74
[18] Ruizi C, Plaja L, Roso L and Becker A 2006 *Phys. Rev. Lett.* **96** 053001